



HAL
open science

An implicit formulation to model the evaporation process in the Eulerian-Lagrangian Spray Atomization (ELSA) framework

Lorenzo Palanti, Stefano Puggelli, Antonio Andreini, Julien Reveillon,
Benjamin Duret, François-Xavier Demoulin

► To cite this version:

Lorenzo Palanti, Stefano Puggelli, Antonio Andreini, Julien Reveillon, Benjamin Duret, et al.. An implicit formulation to model the evaporation process in the Eulerian-Lagrangian Spray Atomization (ELSA) framework. *Atomization and Sprays*, 2020, 29 (12), pp.1043-1069. 10.1615/AtomizSpr.2020032627 . hal-02862478

HAL Id: hal-02862478

<https://hal.science/hal-02862478v1>

Submitted on 27 Sep 2024

HAL is a multi-disciplinary open access archive for the deposit and dissemination of scientific research documents, whether they are published or not. The documents may come from teaching and research institutions in France or abroad, or from public or private research centers.

L'archive ouverte pluridisciplinaire **HAL**, est destinée au dépôt et à la diffusion de documents scientifiques de niveau recherche, publiés ou non, émanant des établissements d'enseignement et de recherche français ou étrangers, des laboratoires publics ou privés.



Distributed under a Creative Commons Attribution - NonCommercial 4.0 International License

An implicit formulation to model the evaporation process in the Eulerian-Lagrangian Spray Atomization (ELSA) framework

L. Palanti¹, S. Puggelli¹, A. Andreini¹, J. Reveillon², B. Duret², & F.X. Demoulin²

¹Department of Industrial Engineering (DIEF), University of Florence, Florence, Italy

²CORIA-UMR 6614, Normandie University, CNRS-University and INSA of Rouen, Saint-Étienne-du-Rouvray, France

In the present work, an implicit evaporation model for the coherent structures of evaporating sprays is introduced and validated against experimental data of engine combustion network (ECN) spray A. The main aim is to go beyond the limits of standard evaporation models, which are normally based on a dilute spray assumption, and develop a strategy to deal with liquid volume fraction virtually up to one. The proposed method is based on a priori computation of the steady-state equilibrium conditions reached by a system composed by liquid, vapor and air at constant pressure combined with a modeled characteristic time of evaporation. Such equilibrium composition and temperature are then used inside numerical calculations to compute evaporation source terms implemented in an implicit fashion. The new formulation allows simulating evaporation process in the dense zone of the spray, where, due to the extremely low time scales related to mass and heat transfer, classical explicit method usually leads to non-physical results. Such innovative approach has been implemented in a multiphase solver based on the Eulerian-Lagrangian Spray Atomization (ELSA) model in the framework of the computational fluid dynamics (CFD) suite OpenFOAM[®]. The use of ELSA allows the mass and heat transfer terms to be modeled as a function of the transported amount of liquid-gas interface surface available for evaporation. An analysis of the model performances has been carried out in an URANS framework in order to highlight the physically consistent representation of evaporation phenomena of the approach in the regions characterized by a high liquid volume fraction.

KEY WORDS: CFD, sprays, evaporation, dense spray region, Eulerian-Eulerian, ELSA, ECN Spray A

1. INTRODUCTION

Spray evaporation is a relevant topic in many technical applications, ranging from diesel engines and aircraft gas turbines to metal cooling and fire suppression system. In all these contexts,

the computational fluid dynamics (CFD) can help to predict the performances of the employed atomization device and to investigate the evaporation that occurs whenever a spray is injected into a hot environment. Liquid evaporation is observed to occur in all the characteristic regions of the spray. In fact, even if most of the mass transfer is expected in the dispersed region, due to the larger amount of liquid/gas interface available, relevant evaporation might also affect the dense region of the spray. The development of a general approach to model liquid phase evaporation in both the dense region and the dispersed one is the main subject of this work.

A typical example is the behavior of the spray in diesel engines, where the fuel is injected during the combustion phase for each power stroke of the piston (Lefebvre and McDonell, 2017). The mixing between fuel and air is accomplished as the continuous jet of fuel, emerging from the orifice of the nozzle, moves at high velocity into the ambient air. Here, the presence of strong disruptive forces gives rise to oscillations and perturbations, eventually leading to the disintegration of the liquid body into drops at its outer edges. At this point, the spray is composed of a solid-cone jet of fuel on the orifice axis (dense region) surrounded by smaller drops of fuel mixed with air (dispersed region) (Lefebvre and McDonell, 2017). Such cone progressively atomizes, generating a cloud of small droplets. Evaporation of fuel takes place throughout the entire process of atomization and a not-negligible amount of fuel evaporates in the early dense region of the spray.

The region of the spray where the investigation is requested to focus, strongly affects the approach which has to be used to track the evolution of the spray and therefore also the associated evaporation model. For instance, standard Eulerian–Lagrangian (E–L) approaches (Bird, 1994) can be effectively used to simulate spray secondary breakup and evaporation in its dispersed region. For this purpose, several sub-models have been developed based on the assumption of a single isolated droplet [i.e., for drag (Haider and Levenspiel, 1989; Liu et al., 1993; Morsi and Alexander, 1972)] or secondary breakup (O’Rourke and Amsden, 1987; Reitz and Beale, 1999; Taylor, 1950): such idea allows a straightforward introduction of the main interactions between the gas and the liquid phase. Nevertheless, the most important shortcoming of E–L approaches is the not-reliable description of the atomization, including therefore a poor representation of the associated evaporation process and of the interface instabilities leading to the breakup of the jet. On the contrary, Eulerian–Eulerian (E–E)-based methods have been traditionally employed to describe the dense region of the spray even if not all of them have been specifically developed to work in this framework. For instance the multifluid models (Laurent and Massot, 2001), the method of moments (Frenklach, 2002), and high-order models such as the quadrature method of moments (QMOM) (Yuan et al., 2012) have been developed to solve a simplified version of the so-called Williams Equation (Williams, 1958) and therefore are not suitable to describe the coherent structures of liquid in the near region of the injector. Essadki et al. (2018) introduced the concept of geometrical high-order moment, that can potentially lead to the extension of such kind of approach to the description of coherent liquid structures. Interface geometry statistics such as interface area density, Gauss curvature, and mean curvature are used at this aim, while evaporation is taken into account using a maximum entropy reconstruction (Essadki et al., 2018).

Usually, an accurate simulation of the primary breakup region can be achieved through a full resolution of the liquid/gas interface by direct numerical simulations (DNS) (Lebas et al., 2009; Ménard et al., 2007; Shinjo and Umemura, 2010, 2011) but its application is currently unfeasible for practical purposes due to the high computational effort required by this kind of approach. Nevertheless, evaporation and simultaneous breakup of sprays have already been investigated in literature coupled with interface capturing method in a DNS context (Duret et al., 2012, 2018; Rueda Villegas et al., 2016; Tanguy et al., 2007). In this line, multi-scale methods have been proposed aiming at extending the capabilities of DNS, by directly simulating the major liquid

structures, whereas Lagrangian tracking is automatically adopted when a proper description of the interface can no longer be provided (Estivalèzes et al., 2018). In this latter case, the use of adaptive mesh refinement (AMR) has proved to be a valid help in optimizing the handling of VOF to E–L transition. Primary breakup has also been recently investigated using the so-called smoothed particle hydrodynamics (SPH) technique. SPH is an interesting alternative method to describe this kind of phenomena (see for instance the work of Braun et al., 2019), mainly because of its superior scalability with respect to traditional approaches. Such method also proved to be suitable for handling evaporation as reported by Yang et al. (2019). Nevertheless having an accurate description of surface tension forces remains a challenging task in SPH formalism and the method’s consistency and convergence remains to be proven. Moreover, the application of this approach to practical evaporating sprays has not yet been attempted. Another opportunity is represented by a group of Eulerian–Eulerian (E–E) methods based on the assumption of diffused interface (Vallet and Borghi, 1999). In this formalism, the interface is represented as a mixing zone where both liquid and gas phases coexist at the same macroscopic location where the portion of volume occupied by the liquid phase is called liquid volume fraction (α_l). Several models have been developed in technical literature under this assumption [for instance Drew and Passman (1999) or the recent work of Battistoni et al. (2019)] and in the following analysis the Eulerian-Lagrangian Spray Atomization (ELSA) model will be considered (Anez et al., 2019; Lebas et al., 2009; Vallet and Borghi, 1999).

In the original ELSA approach, an Eulerian mixture model is used in the near-nozzle region, whereas Lagrangian tracking is employed when the spray becomes sufficiently dilute. Such approach has been validated on some spray configurations (Lebas et al., 2009; Vallet and Borghi, 1999) and its capabilities extended to consider the strong momentum exchange between liquid and gas phase in the so-called quasi-multiphase Eulerian (QME) approach (Andreini et al., 2016; Beau, 2006). Recently the approach has been coupled with an interface capturing method (ICM) (Anez et al., 2019) to more consistently describe the spray formation process also where available mesh resolution allows a full reconstruction of the liquid/gas interface in a large-eddy simulation (LES) context. However, in the mentioned contributions only spray atomization is of primary interest, while, when employed, the modeling strategy for the evaporation process is directly derived from laws developed for a single isolated droplet (Sirignano, 1999). In Lebas et al. (2009) evaporation in the dense zone is not accounted, whereas in Ning et al. (2007) an explicit formulation is applied in the Eulerian region of ELSA and the evaporation rate is computed starting from the local temperature and considering the fuel as saturated on the liquid surface. As it will be shown later, explicit formulation may be unstable and can lead to strong temperature undershoots on the gas side in regions where α_l is really high (i.e., close to the atomizer nozzle).

To overcome the abovementioned limitations of the commonly adopted evaporation model used in the different ELSA-based approaches, a novel implicit formulation has been developed and implemented. This new method permits one to robustly include a general purpose evaporation in ELSA, avoiding at the same time the possible nonphysical behavior in the dense spray region. Such implicit approach is based on a *a priori* calculation of a local equilibrium composition established between the fraction of liquid and gas that coexist in the same control volume. Such composition at equilibrium is then used to compute the evaporation rate. Other approaches based on an implicit formulation have been presented (Desantes et al., 2016; García-Oliver et al., 2013; Kösters and Karlsson, 2011, 2016) and will be discussed in detail in the next sections.

The present modeling strategy has been implemented in the framework of the open source code OpenFOAM[®] and tested on a realistic configuration such as the engine combustion network (ECN) Spray A test case (ECN, 2012). Despite that, the proposed model can be effectively

employed in any configuration where relevant evaporation takes place simultaneously to the primary stages of the breakup process. Being here the attention mainly focused on the dense zone of the spray where the effectiveness of the new model can be properly tested, only the mixture model component of the ELSA approach has been considered. The present approach, even if theoretically extensible also to Lagrangian tracking, does not provide any major improvement when the spray is sufficiently diluted with respect to standard methods. When ICM coupling is considered (Anez et al., 2019), no consistent modifications are needed to the presented approach, even if such coupling is not here attempted due to the relevant computational effort associated to such approach.

The paper is divided into five main sections: the first one is devoted to the justification of the employed numerical framework (i.e., the ELSA approach). In Sections 2 and 3 the limitations of explicit approaches are depicted and the structure of the implicit model outlined. The last two sections are instead focused on the validation of the model, firstly on a simplified 1D test case of an evaporating array of droplets and finally on a realistic configuration representing a diesel spray injector.

2. ELSA SOLVER

Starting from the recent implementation of the ELSA model presented in Anz et al. (2019) a version of the solver capable of handling equation of states has been derived and implemented in OpenFOAM®, in order to deal with heat transfer and evaporation. As a main difference from Anz et al. (2019), the coupling with ICM and Lagrangian tracking have been dismissed, maintaining only the E–E part of the ELSA method characterized by a diffused interface approach. This permitted to greatly simplify the implementation of the evaporation model. No theoretical issues prevent the implementation of the proposed model in the complete ELSA framework. Moreover, the turbulent liquid flux has been modeled with a standard gradient closure but also the second-order strategy developed by Andreini et al. (2016) can be easily introduced in the model. For the sake of clarity, hereafter liquid, vapor, and air will be referred to the subscripts l , v , and a , respectively, while the subscript g will be used for the gas phase fraction composed by both air and vapor. Through all this work an approach based on volume fractions has been employed: the liquid volume fraction will be referred as α_l , the vapor volume fraction as α_v and the air volume fraction as α_a (computed as $\alpha_a = 1 - \alpha_l - \alpha_v$). In the same way, α_g stands for the liquid volume fraction of vapor and air (therefore $\alpha_g = 1 - \alpha_l = \alpha_a + \alpha_v$). For brevity, the detailed derivation of the implemented equations is not carried out at this stage and all of them are directly reported in their final form after Reynolds averaging procedure. However, when combustion is taken into account, Favre averaging would be preferable and will be considered for future developments of the approach. The reader interested in further detail about Favre/Reynolds averaging in multiphase flows is addressed to Anz et al. (2019). The derived set of equations is therefore applicable in a slightly compressible environment, where density variation due to local values of temperature and pressure are accounted using separate equations of state for each component. The proposed compressible solver is still based on a mixture model assumption as the standard ELSA model, therefore a single momentum equation is shared between all the phases [see Eq. (1)].

$$\frac{\partial \bar{\rho} \bar{U}_i}{\partial t} + \frac{\partial \bar{\rho} \bar{U}_i \bar{U}_j}{\partial x_j} - \frac{\partial}{\partial x_i} \left[\mu_t \left(\frac{\partial \bar{U}_i}{\partial x_j} + \frac{\partial \bar{U}_j}{\partial x_i} \right) \right] = \bar{\rho} g_i - \frac{\partial \bar{P}}{\partial x_i} \quad (1)$$

where U represents the averaged mixture velocity, μ_t the turbulent viscosity, g and P gravitational acceleration, and static pressure, respectively. The mixture density can be obtained as $\bar{\rho} = \bar{\alpha}_l \bar{\rho}_l + \bar{\alpha}_v \bar{\rho}_v + \bar{\alpha}_a \bar{\rho}_a$, where bulk densities of vapor and air depend on temperature and pressure, while liquid density is imposed as constant and equal to 713 kg/m^3 . The continuity equation can be expressed as follows:

$$\frac{\partial \bar{\rho}}{\partial t} + \frac{\partial \bar{\rho} \bar{U}_i}{\partial x_j} = 0 \quad (2)$$

A transport equation for vapor volume fraction is included together with the one for liquid. Both of them are solved in a compressible manner and source terms due to evaporation have been added.

$$\frac{\partial \bar{\rho}_l \bar{\alpha}_l}{\partial t} + \frac{\partial \bar{\rho}_l \bar{\alpha}_l \bar{U}_i}{\partial x_i} = \frac{\partial}{\partial x_i} \left[\left(\bar{\rho}_l D_l + \frac{\mu_t}{Sc_{tl}} \right) \frac{\partial \bar{\alpha}_l}{\partial x_i} \right] - \dot{\bar{\alpha}}_{ev} \quad (3)$$

$$\frac{\partial \bar{\rho}_v \bar{\alpha}_v}{\partial t} + \frac{\partial \bar{\rho}_v \bar{\alpha}_v \bar{U}_i}{\partial x_i} = \frac{\partial}{\partial x_i} \left[\left(\bar{\rho}_v D_v + \frac{\mu_t}{Sc_{tv}} \right) \frac{\partial \bar{\alpha}_v}{\partial x_i} \right] + \dot{\bar{\alpha}}_{ev} \quad (4)$$

where D and Sc_t are laminar diffusivity and turbulent Schmidt number of liquid and vapor. Furthermore, $\dot{\bar{\alpha}}_{ev}$ represents the source/sink term related to the evaporation process that will be discussed in detail in the next section. Energy equations, formulated in terms of temperature T , both for gas and liquid, have been also introduced and are reported below [Eqs. (5) and (6), respectively]. The contribution of evaporation appears as additional source term ($\dot{\bar{T}}_{ev}$).

$$\frac{\partial \bar{\rho}_g \bar{\alpha}_g c_{pg} \bar{T}_g}{\partial t} + \frac{\partial \bar{\rho}_g \bar{\alpha}_g c_{pg} \bar{T}_g \bar{U}_i}{\partial x_i} = \frac{\partial}{\partial x_i} \left(\bar{\alpha}_g \frac{\mu_g}{Pr_{tg}} \frac{\partial \bar{T}_g}{\partial x_i} \right) - \dot{\bar{T}}_{ev} \quad (5)$$

$$\frac{\partial \bar{\rho}_l \bar{\alpha}_l c_{pl} \bar{T}_l}{\partial t} + \frac{\partial \bar{\rho}_l \bar{\alpha}_l c_{pl} \bar{T}_l \bar{U}_i}{\partial x_i} = \frac{\partial}{\partial x_i} \left(\bar{\alpha}_l \frac{\mu_l}{Pr_{tl}} \frac{\partial \bar{T}_l}{\partial x_i} \right) + \dot{\bar{T}}_{ev} \quad (6)$$

where c_p is the specific heat and Pr_t is the turbulent Prandtl number.

Regarding the transport equation of the surface density, the same formulation presented in Anez et al. (2019) has been here retained, non-accounting for density variations:

$$\frac{\partial \bar{\Sigma}'}{\partial t} + \frac{\partial \bar{U}_i \bar{\Sigma}'}{\partial x_i} - \frac{\partial}{\partial x_i} \left[\left(\frac{\nu_t}{Sc_t} \right) \frac{\partial \bar{\Sigma}'}{\partial x_i} \right] = \frac{\bar{\Sigma}}{\tau_t} \left(1 - \frac{\bar{\Sigma}}{\bar{\Sigma}_{eq}} \right) \quad (7)$$

where $\bar{\Sigma}'$ indicates the fluctuating component of the overall surface density $\bar{\Sigma} = \bar{\Sigma}_{min} + \bar{\Sigma}'$, where $a \bar{\Sigma}_{min} = 2.4 \sqrt{\alpha_l (1 - \alpha_l)}$, and a is a length scale related to the control volume (Anez et al., 2019). The sink term due to evaporation has been here neglected based on the assumption that, in the dense spray region, turbulent breakup is the dominant phenomenon while evaporation has a minor impact.

In the following, the attention is mainly focused on the method proposed for the calculation of the evaporation source terms.

3. LIMITS OF STANDARD EXPLICIT METHODS FOR DENSE SPRAY REGIONS

The common assumption of spherical droplets is not verified at all in the dense zone of the spray. In fact, while primary breakup takes place, the liquid phase exists as a main coherent structure

and smaller but non-spherical entities like ligaments (Fig. 1). When the atomization quality is poor, for instance in low Weber/Reynolds number condition (Lefebvre and McDonell, 2017), the impact of fuel evaporation from such coherent structures severely affects the flow field (or even combustion for example). Under these conditions, standard Eulerian–Lagrangian approaches based on explicit formulations for evaporation source term can be reliably applied only for low liquid volume fractions. An artificial reduction of liquid volume fraction, by increasing the size of the mesh around the injection point, can be considered as a solution (Abraham and Pickett, 2010), albeit a lower resolution in the Eulerian field is obtained in this way. Indeed, the existence of regions in the domain characterized by high α_l cannot normally be avoided. In this particular zone, which is the main interest of the current work, explicit formulations can be numerically unstable if the simulation time step does not correspond to physical process dynamics, possibly producing non-physical results. Such limits of the explicit methods are discussed using results obtained in a simplified numerical case employing the native Eulerian–Lagrangian solver of OpenFOAM® (i.e., sprayFoam): a single parcel (containing a certain number of droplets) is introduced into the computational domain where it experiences a certain evaporation due to the hot stagnant environment. Liquid temperature is initially set to roughly 40% of the gas phase. On such configuration, it is possible to calculate the temporal evolution of the ratio of ambient gas temperature over liquid temperature for several values of cell liquid volume fraction.

The evaporation source term employed in sprayFoam is based on the following expression:

$$\frac{dm}{dt} = \dot{m} = \pi d \text{Sh} D_g \rho_s \log(1 - X_r) \quad (8)$$

where d is the diameter of the droplet, $\text{Sh} = 2.0 + 0.6\text{Re}^{1/2} \text{Sc}^{1/3}$ is the Sherwood number, D_g the binary mass diffusivity, ρ_s is the gas mixture density at droplet surface, and X_r is the relative molar fraction of vapor surrounding the droplet, computed as $(X_s - X_c)/(1 - X_s)$ where X_s and X_c stand for molar concentration of the evaporating species on the droplet surface and in the carrier phase, respectively. As far as the enthalpy of the liquid is concerned, the heat transfer between gas and liquid, together with the latent heat of vaporization L_v (here assumed constant), compose the sink term:

$$\frac{dh}{dt} = \dot{h} = k A_d (T_l - T_g) - \frac{dm}{dt} L_v \quad (9)$$

where k and A_d stand for the heat transfer coefficient and the droplet surface area. Since both heat transfer and latent heat terms in Eq. (9) become negative under evaporative conditions, undershoots or overshoots in the solution can be generated. From a numerical point of view, this scenario depends on the chosen time step value (dt): lowering dt reduces this effect, but the CPU cost is augmented. In Fig. 2, the ratio between gas phase and liquid temperatures in time

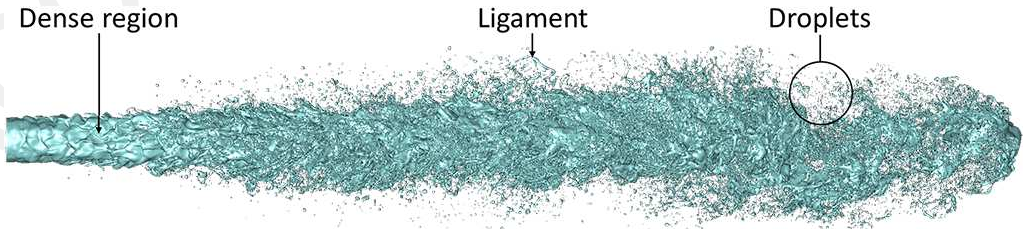


FIG. 1: Diesel-jet direct numerical simulation [adapted from Ménard et al. (2007)]

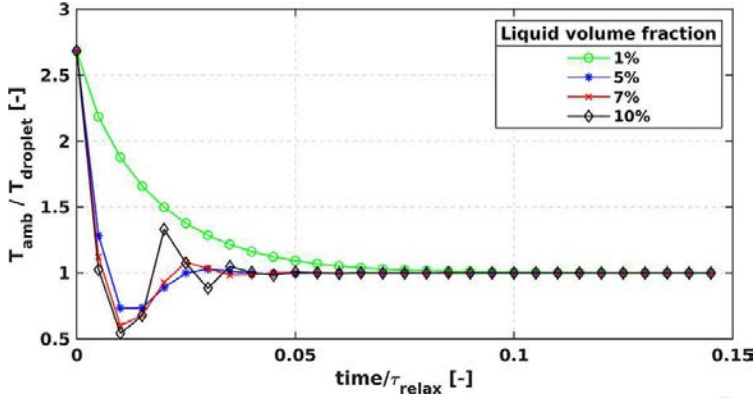


FIG. 2: Ratio of ambient over liquid temperature with respect to time for various liquid volume fraction

is reported for a set of simulations. Dimensionless time is computed using the employed time step and the thermal relaxation time to equilibrium $\tau_{relax} = \rho_s c_{pl} d^2 / (12 k_g)$ (Kinzer and Gunn, 1951), where c_{pl} and k_g are the specific heat at constant pressure of the liquid and the thermal conductivity of the environment, respectively. Different liquid volume fractions are achieved by varying the number of drops inside the parcel, maintaining constant the droplet size as well as τ_{relax} . Generally speaking, during the evaporation process the liquid is heated up and the gas phase is cooled down until a steady evaporation temperature is reached. Under certain conditions, the overall enthalpy of the gas phase is not sufficient to promote complete liquid vaporization because of the energy subtracted by the latent heat. Such final (or equilibrium) condition is always reached in this test case as shown in Fig. 2 at least after 0.1 non-dimensional time, well before the predicted τ_{relax} (because it does not account for the cooling of the gas phase). Before reaching this state, from a physical point of view, liquid temperature should always be lower than the one of the ambient gas and therefore $T_{amb}/T_{droplet} > 1$. But, considering the reported numerical configuration, it is quite clear that such physical constraint is not always respected. In fact, by increasing the liquid volume fraction, the explicit formulation leads to unbounded values of gas-phase temperature. Indeed, as soon as dm/dt is calculated [Eq. (8)] and temperatures are fixed, depending on dt , a certain value of dh is computed through Eq. (9). If dt is not sufficiently small, dh may be large enough to determine a sharp decrease of gas-phase temperature. Hence, temperature undershoots can be observed. Clearly, this issue can be mitigated by reducing the simulation time step, but with a strong increase of the computational cost. In Fig. 3 the $\alpha_l = 5\%$ case has been simulated with two different time steps. The use of a lower time step effectively reduces the numerical issues but CPU cost is increased dramatically, requiring thousands of time steps to simulate the physical timeframe τ_{relax} . Starting from this preliminary observation, it can be concluded that approaching the dense spray region (i.e., $\alpha_l \rightarrow 1$), the time step should be strongly decreased (i.e., $dt \rightarrow 0$) to overcome numerical instabilities with explicit methods. Therefore, considering that one of the main advantages of the ELSA approach is being able to deal both with dense and diluted spray regions, the main purpose of this work is to define a method capable of handling evaporation in the whole evolution of the spray, from pure liquid to the dispersed phase, without any condition on time step dictated by the stability of the evaporation law. As already explained, the attention is hereafter mainly focused on the dense region (Fig. 1) since in the Lagrangian context several evaporation models are already available (Sirignano, 1999) and extensively validated.

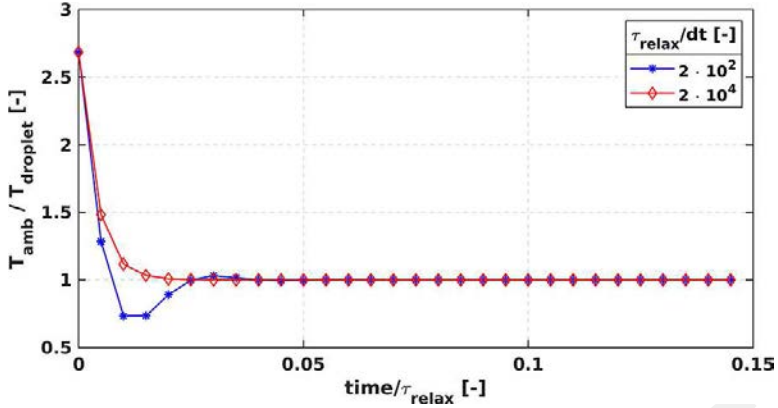


FIG. 3: Ratio of ambient and droplet temperature with respect to time for different time step in Lagrangian simulation

4. IMPLICIT METHOD FOR EVAPORATION MODELING

In the proposed implicit approach, source terms due to mass and heat transfer in Eqs. (3), (4) and Eqs. (5), (6), respectively, have been formulated as reported below:

$$\dot{\alpha}_{ev} = \left(\frac{\alpha_l - \alpha_{l,eq}}{\tau_m} \right) \quad (10)$$

$$\dot{T}_{ev} = \left(\frac{T_{eq_l} - T_l}{\tau_T} \right) \quad (11)$$

where $\alpha_{l,eq}$ and T_{eq_l} represent the equilibrium state reached locally by the liquid/gas mixture in terms of remaining liquid volume and temperature, with two characteristic times defined by τ_m and τ_T . A similar formulation should be employed also for the gas phase in terms of temperature, which is not reported here for the sake of brevity.

Equations (10) and (11) lead to an unconditionally stable system from a mathematical point of view, even if a proper calculation of equilibrium state and evaporation rates has to be provided computing equilibrium liquid volume fraction and temperature with a proper τ .

4.1 Definition of Phase Equilibrium

Different equilibrium conditions can be determined in physics and engineering, going from thermodynamic equilibrium to static equilibrium of bodies. In this study, the word equilibrium refers to the phase equilibrium that can take place between liquid and gas that coexist in the same control volume.

The equilibrium state of a system at a defined temperature and pressure is theoretically provided by the minimum of the Gibbs function (Cengel and Boles, 2015) and the equilibrium conditions, required in Eqs. (10) and (11), can be computed by a direct numerical minimization of this function. This procedure is normally employed to calculate the chemical and the phase equilibrium of complex chemical processes (Gautam and Seider, 1979; Reynolds, 1986).

In this work a different strategy has been adopted, considering the evaporation process that takes place into a two-phase, two-component system inside an isolated control volume at constant pressure. When mass transfer takes place from liquid to vapor phase and vice versa, it is

possible to calculate the equilibrium temperature of the system as (Moran and Shapiro, 2009):

$$T_{eq} = \frac{m_a c_{p_a} T_a + m_l c_{p_l} T_l + m_v c_{p_v} T_v - (m_{veq} - m_v) L_v}{m_{a,eq} c_{p_a} + m_{l,eq} c_{p_l} + m_{v,eq} c_{p_v}} \quad (12)$$

Such equation simply states that enthalpy is conserved over the control volume and also the contribution of the latent heat of vaporization has been here included. To derive it, specific heat coefficients have been considered as constant. This represents one of the main hypotheses of the present procedure. Clearly, variations with temperature should be included, in particular in reactive test conditions, and further investigations are required on this point.

Equation (12) can be further simplified. In fact, mass transfer is not allowed for air ($m_a = m_{a,eq}$) and vapor and air have to share the same temperature T_g before achieving the equilibrium. It can be therefore reformulated as

$$T_{eq} = \frac{m_a c_{p_a} T_g + m_l c_{p_l} T_l + m_v c_{p_v} T_g - (m_{veq} - m_v) L_v}{m_a c_{p_a} + m_{l,eq} c_{p_l} + m_{v,eq} c_{p_v}} \quad (13)$$

which represents the expression of the equilibrium temperature of a two-phase, two-component system subjected to evaporation. However, another relation is required to estimate m_{veq} . According to Cengel and Boles (2015), phase equilibrium of a liquid/air system is reached when the vapor pressure in the air is equal to the saturation pressure of liquid at the liquid temperature. The following relation can be therefore introduced:

$$p_v = p_{sat}(T_{eq}) \quad (14)$$

where p_{sat} represents the saturation pressure that can be computed through relation such as the Antoine equation (Cengel and Boles, 2015) based on experimental measurements. Even a more general Clausius–Clapeyron equation could have been used here, but Antoine equation has been preferred to facilitate future developments of the solver. The partial pressure of vapor (p_v) can be instead expressed in terms of the number of moles of air and vapor in the fraction of volume available for the gas phase.

$$p_v = \frac{n_v}{n_v + n_a} p \quad (15)$$

Hence, equilibrium conditions can be computed varying m_{veq} , until Eq. (14) is satisfied. An iterative cycle has been defined to this end, since p_v directly depends on n_v and therefore m_{veq} while p_{sat} uses T_{eq} computed via m_{veq} .

4.2 Computation of Equilibrium Conditions

In Fig. 4 the code employed for the computation of the equilibrium state is presented (Puggelli et al., 2017). The calculation is carried out in each control volume where a non-zero amount of liquid is observed and the input variables are directly obtained from the numerical simulation. The iterative cycle is based on $m_{l,eq}$, since it can be easily converted in terms of liquid volume fraction using densities while requested phase properties are directly obtained from the numerical simulation in each cell. First of all, the saturated condition is evaluated considering $m_{l,eq} = m_l$, which means that mass transfer does not take place. T_{eq} is calculated by Eq. (13), p_{veq} by Eq. (15), and $p_{sat,eq}$ using Antoine equation for chosen liquid/vapor mixture. If $p_{veq} > p_{sat,eq}$, no further evaporation is allowed. In this case, only heat transfer is included

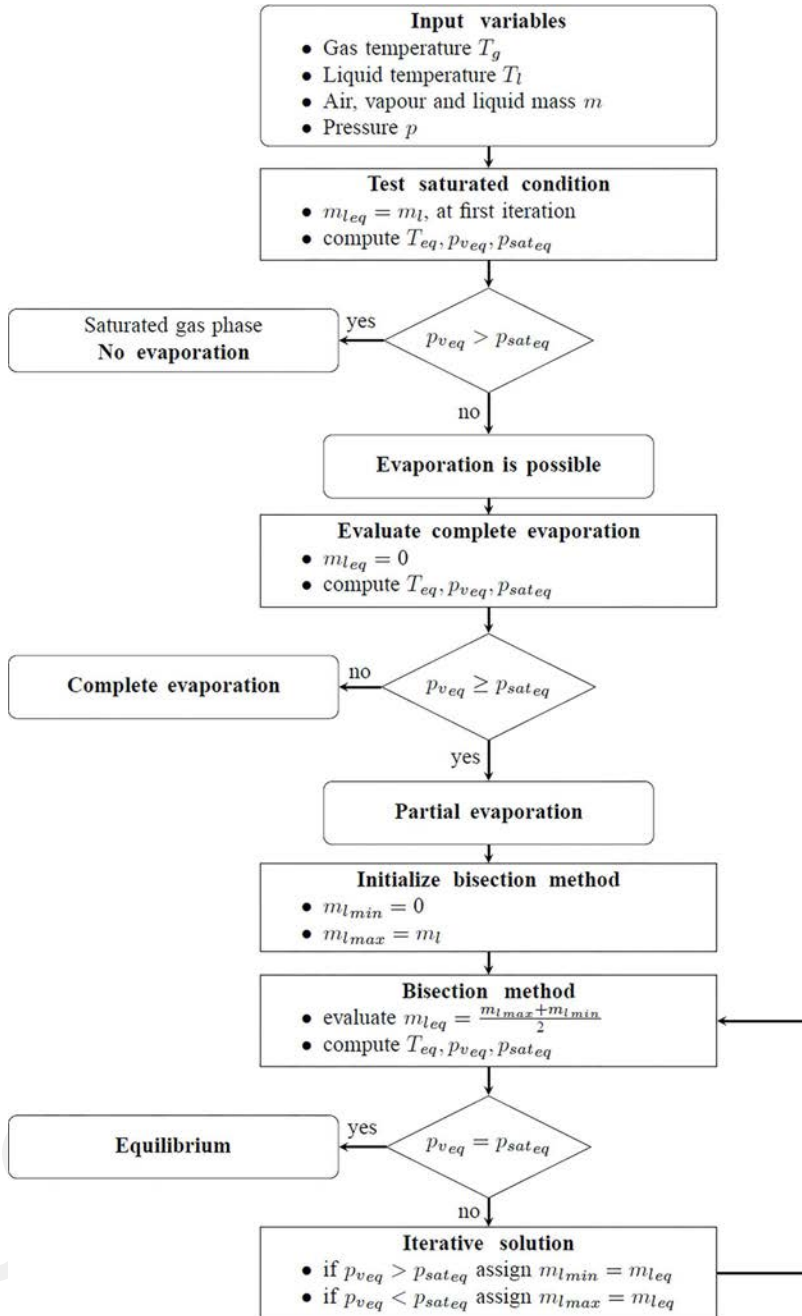


FIG. 4: Method implemented for the computation of equilibrium composition and temperature

between phases and a proper T_{eq} is calculated. On the contrary, if additional evaporation is possible, the case of complete evaporation is evaluated (i.e., $m_{leq} = 0$) and two possible situations are therefore considered:

- if $p_{v,eq} < p_{sat,eq}$ the whole liquid will be evaporated and the final equilibrium temperature for the liquid is set equal to the wet bulb value (see Fig. 5 for further detail), whereas the one for the gas is computed thanks to Eq. (13).
- if $p_{v,eq} \geq p_{sat,eq}$ only partial evaporation takes place. This situation leads to an iterative cycle based on Eq. (14) and, in the present study, a simple bisection method has been employed because of his stability and boundedness. Further developments are surely required on this point to decrease the overall computational effort.

The computed $m_{l,eq}$ and T_{eq} are finally used to compute source terms in Eqs. (10) and (11).

If a complete evaporation is predicted, the equilibrium temperature calculated with Eq. (13) is no more correct at least for the liquid. In fact, the evaporation history of a single isolated droplet (Chin and Lefebvre, 1985) is usually divided in two subsequent steps:

- a heat-up period, when, although evaporation is taking place, the heat transfer from gas to liquid leads to increase the liquid temperature;
- a steady period, when the heat transfer from gas to liquid phase is balanced by the cooling effect of the evaporation. The liquid temperature attains here the wet-bulb value until evaporation is completed.

In this latter period, equilibrium temperatures for gas and liquid are different: the first one reaches the equilibrium temperature determined through Eq. (13), whereas the other one achieves

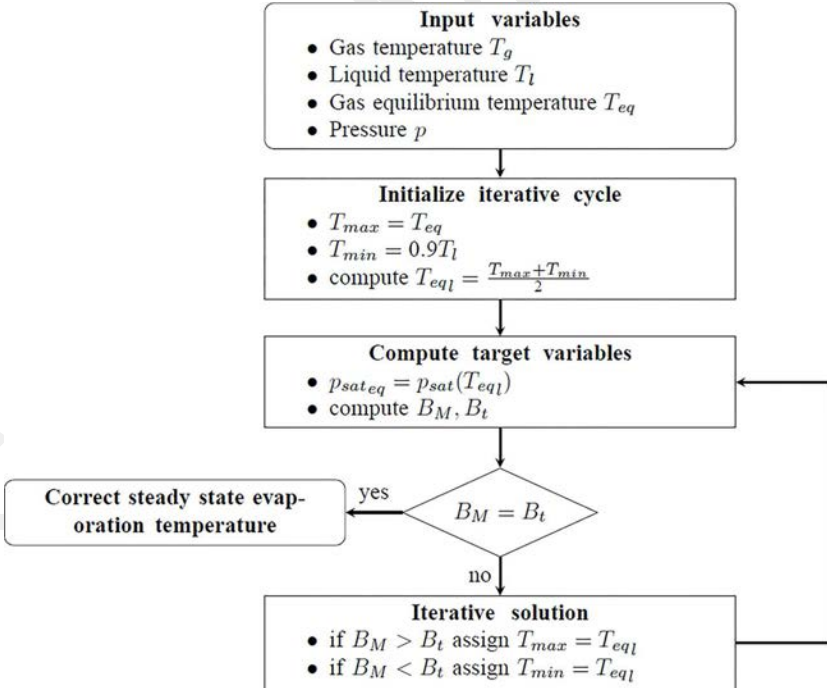


FIG. 5: Method implemented for the computation of equilibrium temperature of liquid in case of complete evaporation

the wet-bulb value. Another iterative cycle has been therefore employed to calculate T_{eq_l} and it is based on the definition of $B_M = (Y_{s,eq} - Y_{g,eq})/(1 - Y_{s,eq})$ and $B_T = [c_{p,g}(T_{eq} - T_{eq_l})]/L_v$ (Lefebvre and McDonell, 2017). $Y_{s,eq}$ is the mass fraction of vapor on liquid surface evaluated using $p_{sat,eq}$ (as a function of T_{eq_l}) while $Y_{g,eq}$ is the one in the gas phase, which can be calculated using $p_{v,eq}$. Note that T_{eq} and $p_{v,eq}$ are already available from the previous cycle. As reported by Lefebvre and McDonell (2017), if $B_M = B_T$, the steady-state period starts and the liquid temperature remains constant until the liquid is consumed. An additional iterative cycle has been developed to determine such constant temperature and is shown in Fig. 5. A bisection method has been again employed. In this manner, a guess value of T_{eq_l} is computed and used to evaluate p_{sat} through the Antoine equation. Then, B_M and B_T are calculated and the two values are compared:

- if $B_M > B_T$, the temperature is reduced
- if $B_M < B_T$, the temperature is augmented

Clearly, the introduction of the numerical procedure presented above requires an additional effort in terms of computational resources. This is almost negligible as it does not involve iterations in the global resolution of the pressure–velocity coupling. The pressure–velocity step, for low-mach methods that are pressure based, requires in particular the resolution of the Poisson equation for the pressure term that is still the most intensive process in terms of CPU usage.

4.3 Computation of Characteristic Time Scales

The remaining parameters that have to be defined to close Eqs. (10) and (11) are τ_m and τ_T . Modeling strategies for the rate of evaporation to be applied all along the atomization process are not yet available in technical literature. To overcome this difficulty, a first solution here employed is obtained recasting the evaporation rate reported by Abramzon and Sirignano (1989). In this way, a proper rate is recovered in the dilute spray region, even if characteristic evaporation time scale is underestimated in the dense part. However, this error should be partially compensated by the implicit method. In fact, the above cycle allows one to properly calculate the equilibrium conditions everywhere and the modeling approximation is only given by τ . Furthermore, in the near-injection regions, the volume left for gas phase is generally small ($\alpha_l \rightarrow 1.0$) and it will be rapidly cooled and saturated by vapor. Therefore, due to the limited amount of liquid that can evaporate, the characteristic time associated with this process will be very small. Hence, if the estimation of the vapor concentration under equilibrium conditions is correct, the evaluation of the time scale employed is considered less important. This observation leads also to the conclusion that, even if with an implicit method the time-dependent evolution cannot be properly resolved, this transient phase should not impact too much on the accuracy of the solution. Further developments are required to calculate the characteristic time scales of evaporation, introducing other geometrical properties of the liquid/gas interface such as the curvature of the liquid surface. The reader interested in this topic is addressed to Canu et al. (2018). Finally, another key point to determine the characteristic time scales is to ensure the coherence between evaporation and heat transfer times. The employed formulation verifies this requirement. Using the equation presented by Abramzon and Sirignano (1989) for \dot{m} , it is possible to obtain the expressions of τ_m and τ_T shown below:

$$\tau_m = \frac{m_{l,eq} - m_l}{\dot{m}} = \frac{m_{l,eq} - m_l}{\pi d n_d S h^* D_g \rho_g \ln(1 + B_M)} \quad (16)$$

$$\tau_T = \frac{T_{leq} - T_l}{(\dot{Q} - \dot{m}L_v)/(c_p m_l)} \quad (17)$$

where the mass Spalding number B_M is computed using the volume fraction of liquid α_l converted into liquid mass fraction. Also d and n_d are calculated from α_l and Σ (Anez et al., 2019):

$$d = \frac{6\alpha_l(1 - \alpha_l)}{\Sigma} \quad (18)$$

$$n_d = \frac{V_{liquid}}{V_{droplet}} = \frac{V_{liquid}}{V_{cell}} \frac{V_{cell}}{V_{droplet}} = \alpha_l \frac{6}{\pi d^3} V_{cell} \quad (19)$$

Equations (18) and (19) are used to recast the evaporation rate in terms of ELSA variables such as α_l and Σ . Such derivation is strictly correct only under the assumption of having a cloud of spherical droplets uniform in size in the same computational cell. This is generally not true in sprays, especially in the regions of primary breakup where in addition to a non-uniform size distribution also ligaments or larger structures can be identified. As stated above, this shortcoming should not strongly affect the prediction of the evaporation in the dense zone, where it is preferable to have a reliable prediction m_{leq} . The so-called modified Sherwood number Sh^* reads

$$Sh^* = 2 + \frac{Sh_0 + 2}{F(B_M)} \quad (20)$$

and

$$Sh_0 = 2 + 0.552Re^{1/2}Sc^{1/3} \quad (21)$$

where $F(B_M)$ is a function of the Spalding mass transfer number B_M (Lefebvre and McDonell, 2017). The Reynolds number, employed in the definition of Sh_0 , is calculated using the fluctuating component of velocity derived from the turbulent kinetic energy (Chin and Lefebvre, 1985):

$$Re = \frac{u'd\rho_g}{\mu_g} \quad (22)$$

Furthermore, in Eq. (17), \dot{Q} , which is the heat transfer between phases, appears and can be calculated as

$$\dot{Q} = \pi d n_d Nu^* k_g \frac{\ln(1 + B_T')}{B_T'} (T_g - T_l) \quad (23)$$

where k_g is the gas thermal conductivity, Nu^* is the corrected Nusselt number to account for the effects of Stefan flow and B_T' is the thermal Spalding number. Under the assumption of $Le = 1$, it is possible to state that $Nu^* = Sh^*$ and $B_T' = B_M$, closing therefore the system of equation. The complete expression of τ_m and τ_T is not reported for the sake of brevity but it can be easily recast from the equations reported above. All these quantities are valid both for the dilute and dense spray regions since they are based only on geometrical properties of the droplet–gas interface, which are defined in the entire domain.

4.4 Comparisons with Similar Published Approaches

Since similar approaches to model evaporation can be found in scientific literature, this section is devoted to highlight the differences between the present work and previous ones available. Kösters and Karlsson (2011) introduced a similar approach to handle the source terms due to the

mutual interaction of air and spray in the framework of the so-called VSB2 spray model. In this work liquid phase is tracked as if composed by blobs (Pilch and Erdman, 1987), namely clusters of droplets with a certain size distribution where all the interactions between the blob and its surroundings take place in a bubble surrounding the blob, rather than the entire computational cell it currently occupies. The standard droplet equations of momentum, mass and energy are replaced with relaxation equations for the blob (Kösters and Karlsson, 2011) where the structure of the source terms is similar to the one reported in Eqs. (10) and (11). In fact, equilibrium values of mass and temperature are computed to ensure the bounding of the solution, while relaxation times are provided to define the rate of change of the considered variable. Equilibrium temperature is calculated assuming an adiabatic mixing, while the remaining mass of liquid under equilibrium conditions is achieved through a fully coupled iterative solution of mass and energy, accounting for the latent heat of evaporation (Kösters and Karlsson, 2011). Evaporation will stop if the gas phase is saturated and the resulting temperature is lower than the critical temperature of the liquid (Kösters and Karlsson, 2016). Additional detail about such coupled iterative solution are provided neither in Kösters and Karlsson (2011, 2016). Despite the totally different approach for liquid phase tracking, in the present work several similarities can be highlighted regarding the idea of ensuring an unconditionally robust solution exploiting an implicit approach based on equilibrium values computed through an iterative procedure to account for the effect of latent heat of evaporation on final temperature, as described in Section 4.2.

In the same line, García-Oliver et al. (2013) and Desantes et al. (2016) proposed an original implementation of evaporation modeling based on local adiabatic saturation conditions in the context of the $\Sigma - Y$ approach. The enthalpy of the mixture is transported within the computational domain to retrieve the local averaged mixture saturation temperature, similarly to Eq. (13), once the local composition is known. Such temperature is finally used to directly compute the local saturation pressure of fuel vapor [as depicted in Eq. (14)], which is later employed to recover the evaporated mass fraction in equilibrium conditions (see Section 4.1). The mass source/sink terms in the vapor/liquid mass fraction equations are in the end expressed as a linear relaxation towards such equilibrium values, as it is done in Eqs. (10) and (11). Due to the absence of internal loops, local mixture temperature at saturation should not account for the evaporated mass since, to the best of author understanding, the value of liquid mass fraction used to calculate such temperature is directly retrieved by the transport equation. Therefore, compared against the strategy presented in the previous sections, here the effect of the latent heat of vaporization on equilibrium temperature is neglected. Strictly speaking, the employed approach is physically consistent only when no evaporation occurs and equilibrium temperature is just related to the adiabatic mixing of components. To underline the effect of the latent heat, the approach described Section 4.2 has been applied to compute the equilibrium conditions starting from different values of initial liquid volume fraction (Fig. 6) including and not including the cooling effect of the phase change [thus using $L_v = 0$ in Eq. (13)]. Here, the considered liquid is n-heptane with an initial temperature of 288 K, while the gas phase is composed of air only (no initial vapor) at 773 K and at ambient pressure. Figure 6 shows that almost no difference can be pointed out for very diluted ($\alpha_l < 10^{-5}$) or very dense ($\alpha_l > 10^{-2}$) sprays. But, an intermediate range exists ($10^{-5} \leq \alpha_l \leq 10^{-2}$) where the effect of latent heat is really strong. For instance, for $\alpha_l = 10^{-3}$ full liquid evaporation is predicted if no latent heat is taken into account, while only partial evaporation takes place if it is considered [Fig. 6(a)]. Also a certain difference in final equilibrium temperature is noticeable [Fig. 6(b)]. This explains the need of taking into account the latent heat of vaporization in the final equilibrium computation when all the possible ranges of α_l have to be investigated. Due to the need of computing the amount of evaporated liquid and the temperature

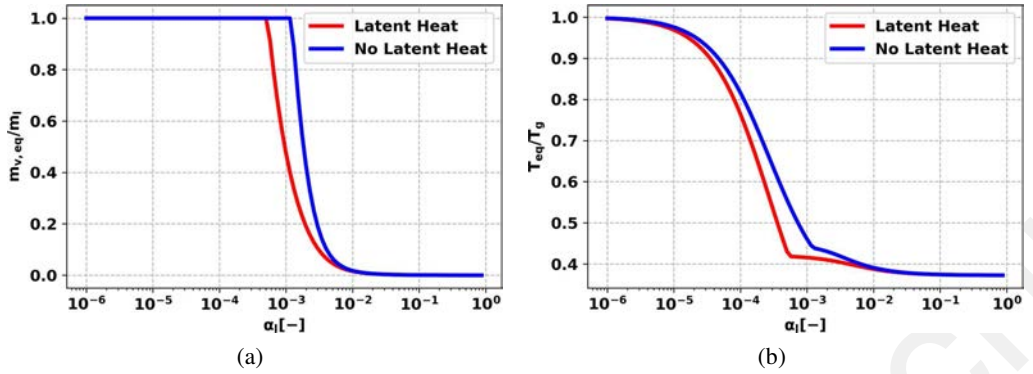


FIG. 6: Ratio of liquid mass converted into vapor at equilibrium (a) and associated equilibrium temperature (b) for different initial liquid volume fractions

in a coupled way, in this work an inner cycle has been introduced and explained in Section 4.2 to predict such thermodynamic equilibrium state without further assumption on the final state of the mixture. A less relevant difference is also represented by the characteristic time scale used in the source terms, once equilibrium conditions are known. In García-Oliver et al. (2013) and Desantes et al. (2016) it is set equal to the physical time step employed in the calculation, meaning that the local thermodynamic steady-state condition is reached within a single time step of the simulation. However, this can affect the prediction of spray evaporation since the particle relaxation time varies inside the domain based on the local flow-field properties. Following the lead of Kösters and Karlsson (2011, 2016), in the present work a more physical derivation from a previous evaporation law is attempted as reported in Section 4.3.

5. VALIDATION OF THE MODEL

Before going into detail with an assessment of the developed solver on the experimental test case studied in the ECN framework, in this section a preliminary theoretical validation of the solver is provided. To this aim, the evaporation process of an n-heptane droplet with a diameter of $20 \mu\text{m}$ is investigated using the ELSA solver and the evaporation model previously presented. A certain amount of liquid is introduced with a temperature of 288 K in a stagnant environment at 773 K and let free to evaporate. The operating pressure is 101,325 Pa while the relative velocity is set to zero. Figure 7 reports the comparison between the theoretical result obtained implementing the iterative method reported by Lefebvre and McDonell (2017) and the one provided by the solver. The dependency of thermo-physical properties on temperature and pressure has not been included. In order to provide a consistent comparison, the initial liquid volume fraction α_l has been set accordingly while the density of interface Σ has been computed assuming a spherical shape of the liquid phase, deactivating its transport equation. A fair agreement can be pointed out: the implemented model is able to correctly represent both the initial period of heat-up and the time evolution during the steady-state evaporation.

6. VALIDATION ON THE ECN CONFIGURATION

The diesel injector, studied in the ECN (2012), has been chosen for the assessment of the proposed approach for evaporation modeling.

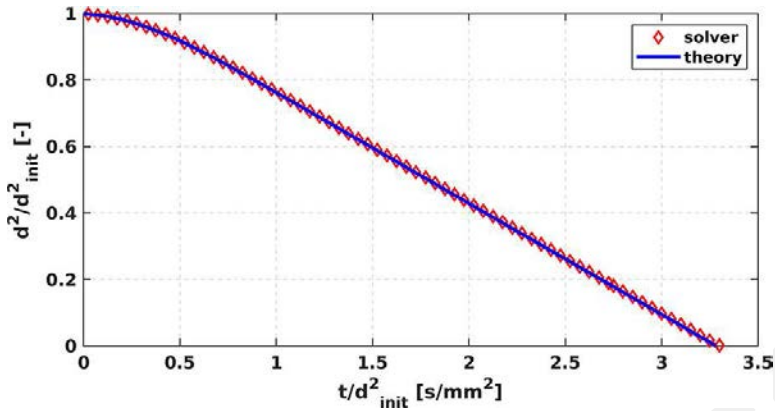


FIG. 7: Analytical validation of the code for a single evaporating droplet

The apparatus is based on a common rail injection system, which is used to supply fuel to a diesel injector. Several operating conditions have been tested and, in the present set of measurements, the rail pressure ranges from 50 to 150 MPa. The spray is injected into an ambient with a density of 22.8 kg/m^3 (i.e., corresponding to $P_{amb} = 6 \text{ MPa}$ and $T_{amb} = 900 \text{ K}$). The injector is fueled with a single component n-dodecane. The nominal diameter of the injector here analyzed is 0.084 mm and the interested reader is addressed to Kastengren et al. (2012) and to ECN (2012) for a detailed description of the experimental test article (i.e., referred as Spray A).

In terms of boundary conditions, the liquid fuel is injected through the nozzle at 363 K with an inlet velocity varying from 300 m/s to about 600 m/s based on the injection pressure. The injected fuel, thanks to the injection velocity and to the high temperature of the combustion chamber, rapidly breaks-up and evaporates. Operating conditions are briefly summarized in Table 1. The reference test point for the present work, named hereinafter as Test point 1, is identified by an injection pressure of 150 MPa. It is surely the most representative and challenging condition and it has been already widely investigated in technical literature (ECN, 2012; Desantes et al.,

TABLE 1: Operating conditions of the simulated configurations, based on data from ECN (2012)

Injector series	210,677 – Spray A
Orifice nominal diameter [mm]	0.084
Injected fuel	n-dodecane
Fuel density [kg/m^3]	713
Fuel temperature [K]	363
Mean injection pressure [MPa]	150, 100, 50
Ambient density [kg/m^3]	22.8
Nominal ambient temperature [K]	900
Ambient pressure [MPa]	6.05
Discharge coefficient	0.89
Area contraction coefficient	0.98

2016). Two further test points, characterized by an injection pressure of 100 MPa (Test point 2) and 50 MPa (Test point 3), have been also considered to further assess the capabilities of the proposed approach. Several experimental data are available on this test case. Mie scattering has been employed to measure the liquid length using a 3% threshold of the maximum intensity. The steady liquid penetration has been also evaluated and it has been obtained by averaging the instantaneous snapshots between 0.5 and 1.4 ms (ECN, 2012; Kastengren et al., 2012).

Rayleigh scattering (ECN, 2012; Kastengren et al., 2012) has been instead used to obtain the distribution of mixture fraction. Instantaneous images have been averaged to compute mean contour plots provided in the ECN database. Data are available starting from 17.85 mm after the injection point until 50 mm downstream. Hence, the ECN test case is particularly suitable to validate the proposed code since a large region, where α_l tends to one, can be found. From a theoretical point of view, this would constrain E–E or E–L solvers, based on an explicit strategy, to strongly reduce the time step size to avoid a non-physical behavior of the evaporation source terms. When a practical case is considered, there are regions where α_g is so small that is likely impossible to stabilize the simulation adopting a feasible time step and therefore the use of an explicit approach must be ruled out. Conversely, the implicit approach should lead to a robust representation of the involved phenomena and the ECN measurements on vapor mass fraction, focused on the near-injection region, are surely adequate for its assessment.

6.1 Numerical Setup

Unsteady Reynolds-averaged Navier–Stokes (RANS) simulations have been carried out on the axi-symmetric domain shown in Fig. 8, representing a 5° sector of the whole domain with 1 element in the azimuthal direction. The axial and radial extensions are smaller than the actual chamber (i.e., 108 mm \times 108 mm against 100 mm \times 20 mm in present calculations). However, it has been verified that this choice has a negligible impact on simulation results. Considering that the focus of this part of the work is on evaporation modeling, the injector duct has not been included and the diameter has been reduced based on the area contraction coefficient (see Table 1). Such assumption allows neglecting the cavitation inside the nozzle, which would affect the real velocity profile, and concentrating the study just on the downstream region. As shown in Hoyas et al. (2013), García-Oliver et al. (2013), and Desantes et al. (2016), where the ELSA approach was used to study the liquid/gas interface for the same test case, a mesh sizing counting 10 elements along the injector diameter is necessary to properly reproduce the main features of the flow field as the liquid–air mixing. A structured mesh counting 12,500 cells with a size of 0.008 mm at the injector exit has been therefore generated. A further refined mesh with a double number of elements in the injector diameter has been also tested to assess the effects of the numerical domain. No appreciable effects of the mesh sizing on the provided results have been pointed out and the coarser mesh has been adopted.

Mass flow rate has been imposed at the injector inlet following the available experimental data, whereas a static pressure has been prescribed at the outlet. All the walls have been considered as smooth, non-slip, and adiabatic, whereas cyclic conditions have been applied on the two lateral patches (see Fig. 8). The employed time step ($d\tau$) has been chosen as much as high without compromising the numerical stability. Therefore, $d\tau = 1.5 \times 10^{-8}$ s for Test point 1, while it has been increased to 1.85×10^{-8} s in Test point 2 and to 2.5×10^{-8} s in Test point 3 thanks to the reduced injection velocity. In all the test points, the chosen $d\tau$ ensures that the Courant–Friedrichs–Lewy (CFL) number is kept below one.

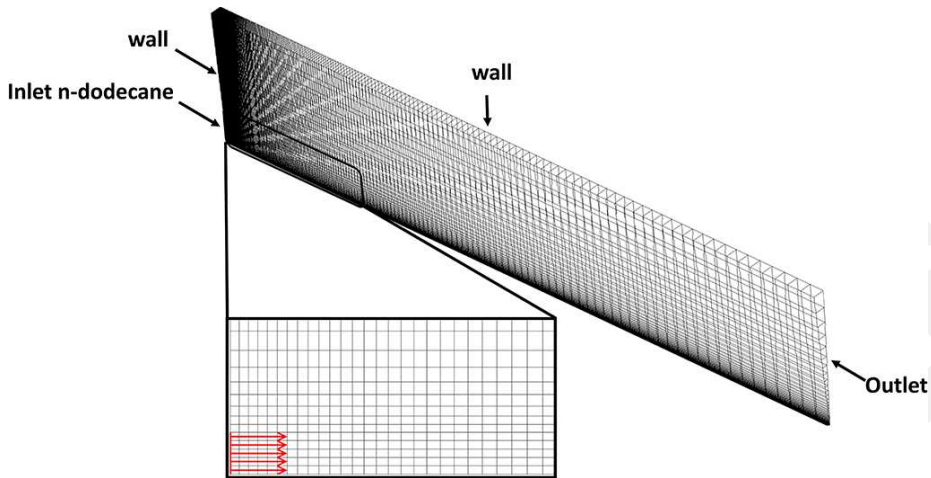


FIG. 8: Employed computational grid and imposed boundary conditions

With regards to turbulence modeling, a standard k - ϵ model has been employed. Both convective and diffusive fluxes have been discretized following second-order schemes, whereas first-order Euler scheme has been employed for time advancement. Finally, in the next section, several results, regarding both liquid length and vapor penetration, are discussed: to this aim a threshold on a certain value of mass or volume fraction is normally used. In this work $\alpha_l = 0.1\%$ and a fuel mass fraction of 0.1% have been used to this end as already done in previous works on the same test case (Kralj, 1995) and as suggested by ECN guidelines (ECN, 2012).

6.2 Results and Discussion

The validation of the evaporation model starts with the simulation of Test point 1. Before starting with quantitative comparisons, Fig. 9 shows velocity and liquid-gas interface density evolution in space together with liquid and vapor fraction contours obtained with ELSA on a window of $10\text{ mm} \times 3\text{ mm}$ after the injector exit. It represents the near-injection region where the breakup mainly takes place. The liquid jet, due to its high Weber and Reynolds numbers, enters into the chamber and undergoes a quick atomization process, which is highlighted by the zone where the production of Σ is really high. Such violent atomization is mainly related to the growth of instabilities on the liquid surface due to the turbulent interactions with the gas phase. However, it is also strongly affected by the heat-up and evaporation of liquid that take place immediately in the near-injection region. A liquid core is therefore generated and the spray tends progressively to evaporate producing a region with a non-negligible volume of n-dodecane vapor. At the end of the selected window, the vapor volume fraction exceeds already the 10% and this can have an important effect on the stabilization mechanism if reacting test conditions would be considered. Furthermore, even in regions where the liquid volume fraction is really high (i.e., $\alpha_l \simeq 0.8$ – 0.9) the code is able to robustly determine a non-zero evaporation rate with a consequent production of α_v . In these regions, it is likely that an explicit method would have present strong numerical instabilities and under-shootings in gas-phase temperature.

To clearly show this limit, the implicit source term of evaporation has been reformulated also in an explicit fashion for Eq. (5). The other aspects of the numerical setup have been retained as

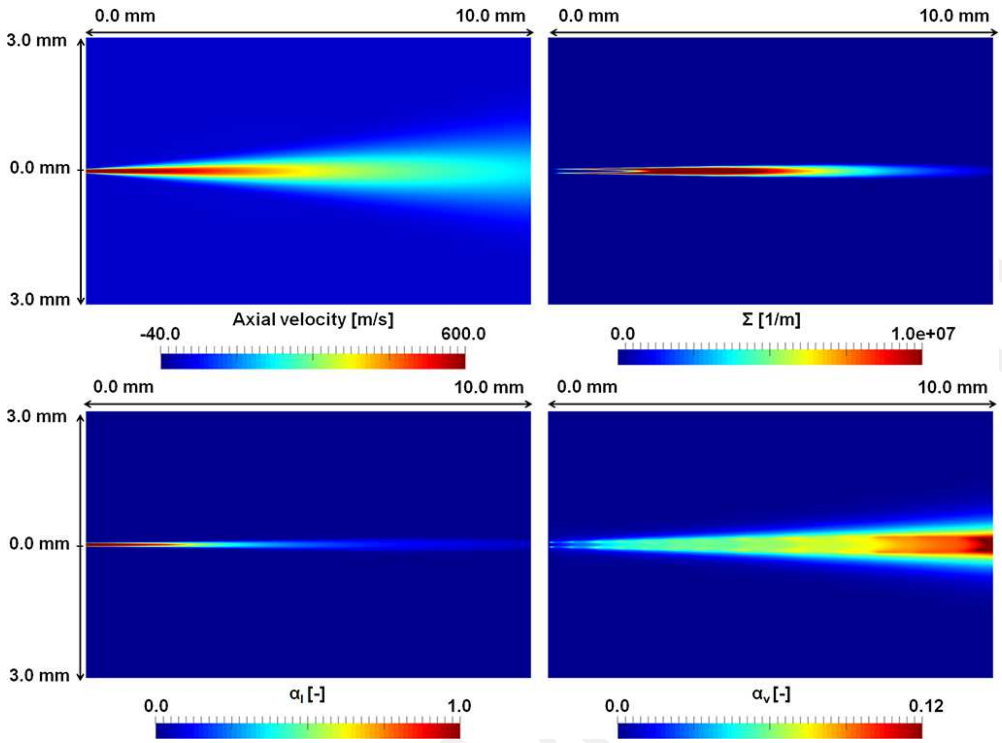


FIG. 9: Mixture velocity, liquid/gas interface density, liquid, and vapor fractions distributions in the dense spray region (in a window of 6.0×10.0 mm)

in Section 6.1. Employing the same time step, in Fig. 10 the minimum value of the ratio T_g/T_l in the domain is reported for both explicit and implicit approaches. Clearly, the issues shown in Section 3 arise again with the explicit methods. A non-physical behavior is predicted and the simulation crashes after few iterations. A robust and stable numerical prediction is instead obtained by using the implicit approach.

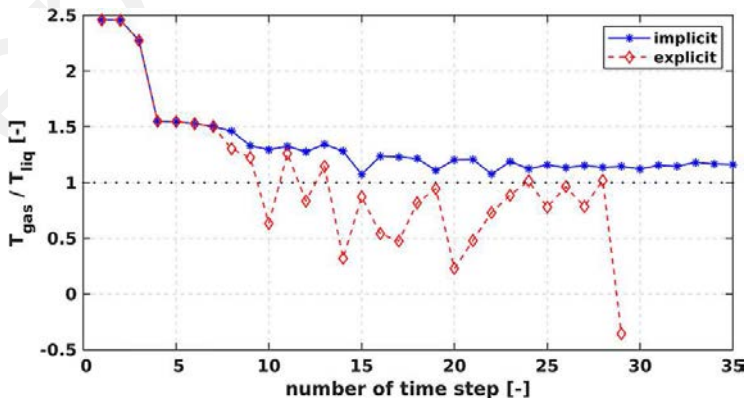


FIG. 10: Instabilities in gas-phase temperature with explicit source term in gas-phase temperature

Going further downstream such dense region, from a quantitative point of view, spray vapor penetration and liquid length evolution are analyzed in Fig. 11 for Test point 1. At this point, the turbulent Schmidt number for vapor has been set to a standard value of 0.7 while the one for liquid has been imposed equal to 1.25 after a tuning process to match liquid penetration, addressing the focus of the validation only on the evaporation rather than on liquid dispersion. Due to the high injection pressure here considered, the vapor penetration grows fast and this is due to the velocity at the injector exit. The instantaneous vapor penetration is related to the momentum flow rate of the liquid emerging from the atomizer. The mass flow rate, the nozzle exit velocity, and the spreading rate of the spray are thus directly affecting such penetration. They also influence the evaporation rate by enhancing the turbulent mixing and the hot ambient gas entrainment in the spray core, again with certain effect on vapor penetration. All these phenomena are observed experimentally and only partially recovered by the numerical model. In fact, a slight under-prediction of vapor penetration can be pointed out, which is probably related to a certain low momentum exchange between vapor and the surrounding air caused by the turbulence model. Considering that a URANS approach with no calibration is here employed, the agreement is considered acceptable for the validation purpose of this section.

Beyond such good agreement in terms of penetration, the mixture fraction distribution has been analyzed as it represents the key point since it is directly related to the evaporation of the liquid fuel. Figure 12 shows the results obtained for Test point 1 in terms of both axial and radial distribution. An overall good agreement has been obtained. The shape of profiles is adequately predicted and in particular the centerline curve agrees well with experimental data. No relevant differences can be pointed out between the fine and the coarse mesh, therefore the latter has been chosen for all the calculations. Considering the resulting contour plots (see Fig. 13), vapor concentration seems to be slightly over-predicted, mainly in the near-axis zone and the difference with experiments tends to decrease going further downstream. At higher axial distances, the effect of turbulence modeling is less pronounced and numerical results properly reproduce the vapor concentration both in terms of axial and radial distributions. Therefore, based on a physical representation of the turbulence flow field and mixing, the developed code is able to properly predict the local equilibrium state and the final vapor concentration. This has been further verified studying the velocity profiles at increasing distances from the nozzle. However, experimental data in terms of flow field were not available for the injector under investigation.

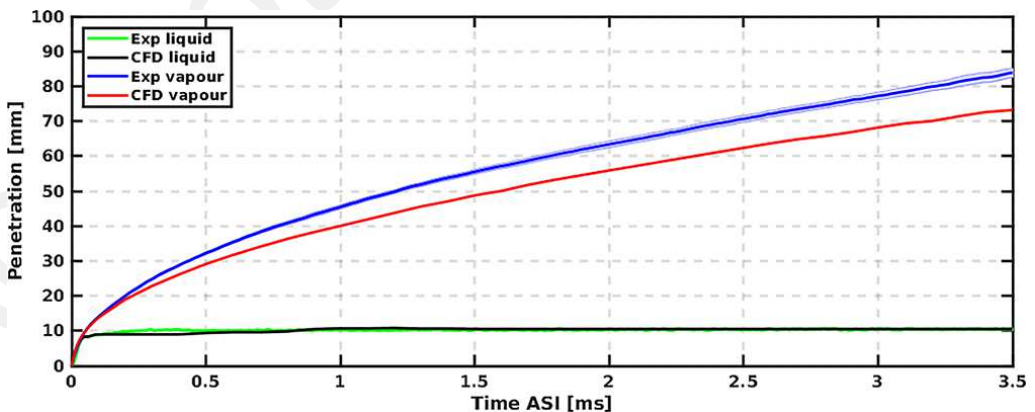


FIG. 11: Computed and measured liquid and vapor penetration for Test point 1

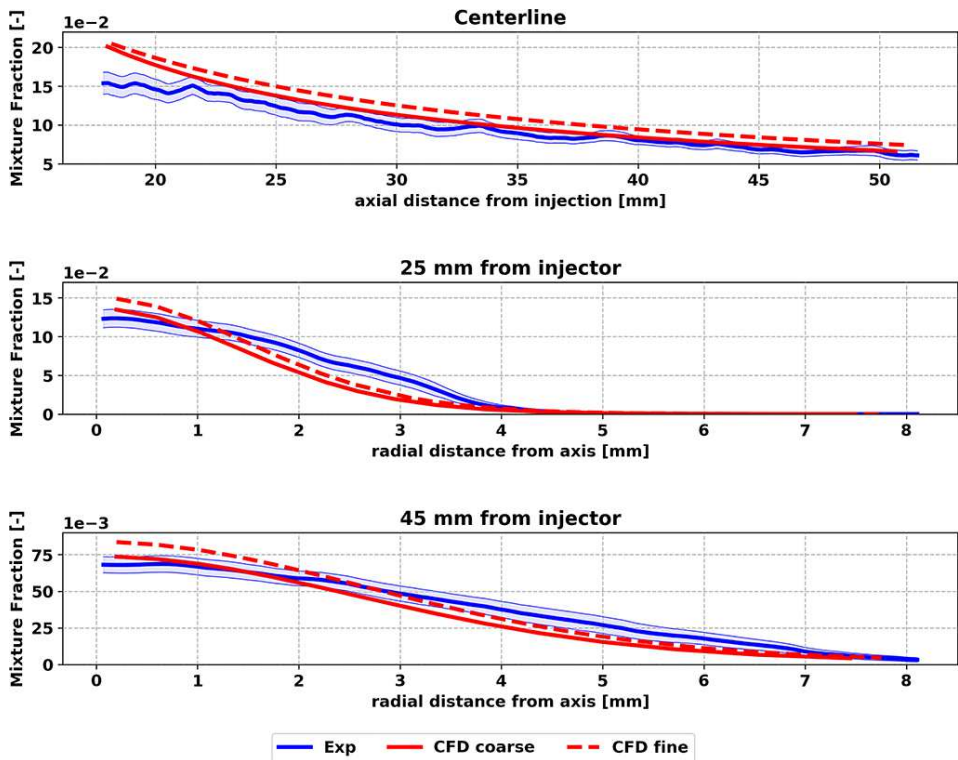


FIG. 12: Mixture fraction distributions for Test point 1

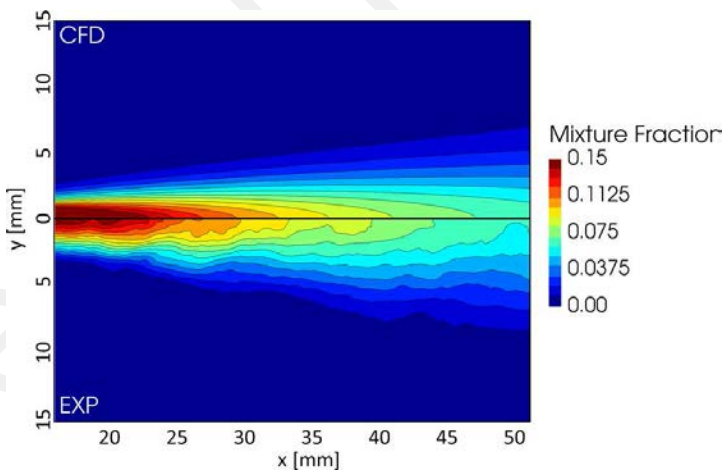


FIG. 13: Mixture fraction contour comparison for Test point 1

Therefore, the comparison shown hereinafter was realized using data of the nozzle 210,678 from Pandal (2016), which was characterized by a hole diameter slightly bigger (i.e., $d = 83.7 \mu\text{m}$ for 210,677 and $d = 88.6 \mu\text{m}$ for 210,678). Hence, in order to make a proper comparison between experiments and CFD, as already done in Pandal (2016), in Fig. 14 radial profiles of

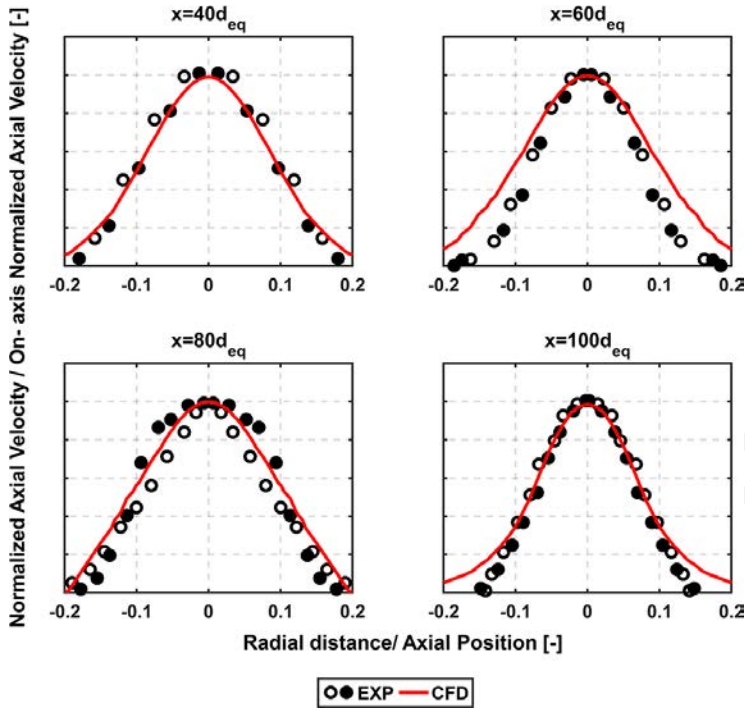


FIG. 14: Comparison between radial velocity profiles normalized at $40d_{eq}$, $60d_{eq}$, $80d_{eq}$ and $100d_{eq}$ between CFD and experiments (empty and full dots come from different sides of experimental acquisition)

axial velocity normalized by the value taken on the axis are plotted at different axial distances using an equivalent diameter as reference length (i.e., $d_{eq} = d\sqrt{\rho_f/\rho_{amb}}$). Note that original experimental points were originally non-symmetric and that they have been doubled and reflected along the y axis to obtain a symmetric distribution for comparison (empty and full dots).

At axial positions, where the numerical approach here employed fails in properly reproducing the jet opening angle (i.e., $x = 60d_{eq} \cong 30$ mm), a low accuracy was reported in the mixture fraction field (see Fig. 12). Conversely, as soon as the distance from the injector is increased a fair agreement is retrieved both in terms of flow field and mixture fraction distributions.

To reduce the impact of turbulence modeling and to focus the attention just on evaporation modeling, Test case 2, which is characterized by a lower injection pressure and liquid velocity, has been considered. The distribution of vapor mass fraction is now well caught on the axis (Fig. 15). Due to the lower turbulence intensity, a more consistent representation of the flow field is obtained and mixture fraction profiles mimic well the experimental evolution both in terms of axial profile and radial spreading. Pressure and velocity fields, together with liquid volume fraction, even in URANS framework, are now correctly reproduced and this leads to properly calculate both the equilibrium state as well as the global evaporation rate. This is confirmed by the overall mixture fraction field shown in Fig. 16. A reliable prediction of vapor distribution can be again pointed out.

To further assess the solver capabilities on another operating condition, Test point 3 has been considered and results are shown in Fig. 17. As also reported for Test point 2, numerical results

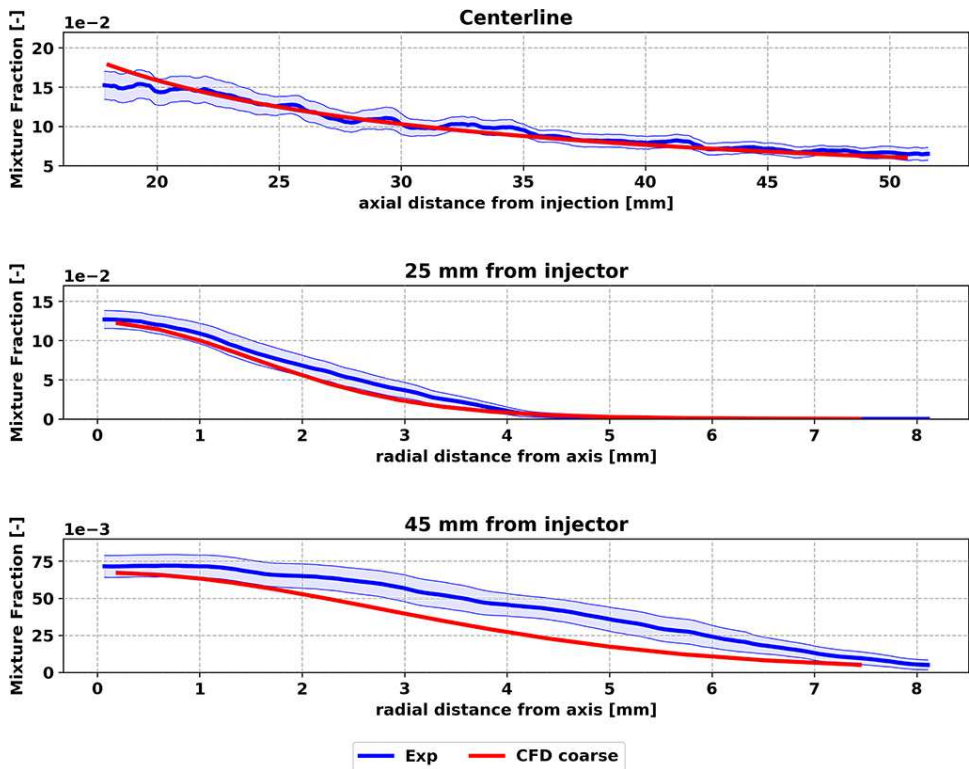


FIG. 15: Mixture fraction distributions for Test point 2

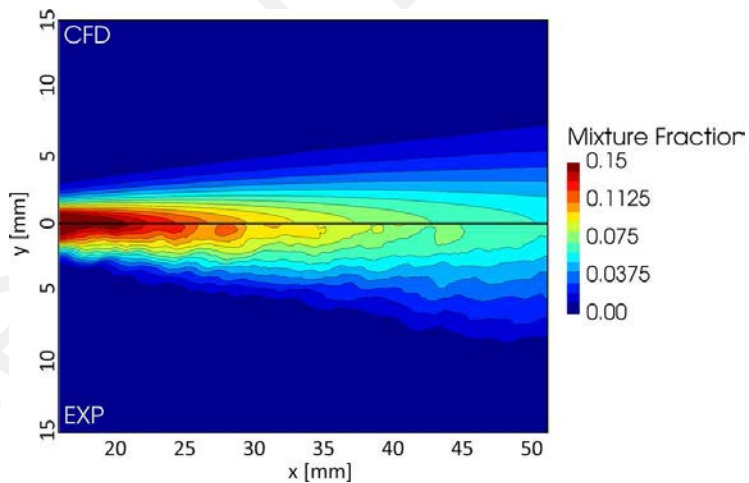


FIG. 16: Mixture fraction contour comparison for Test point 2

agree well with experiments, both in terms of center-line and radial distributions. Contours of the mixture fraction for experiments and numerical simulations are compared in Fig. 18. A really accurate prediction of the vapor evolution is obtained.

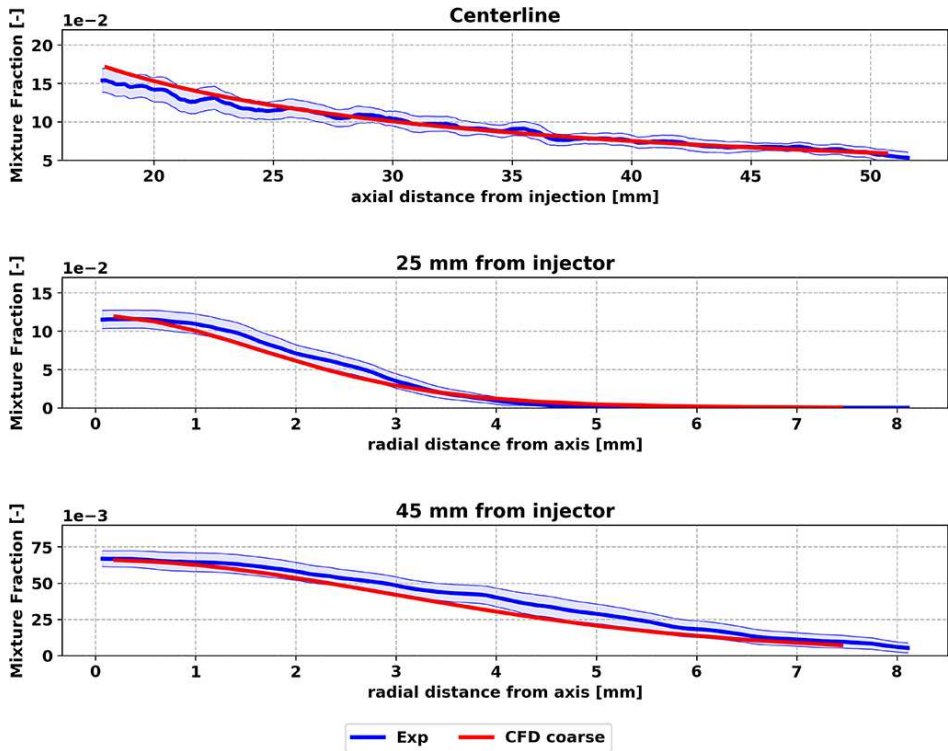


FIG. 17: Mixture fraction distributions for Test point 3

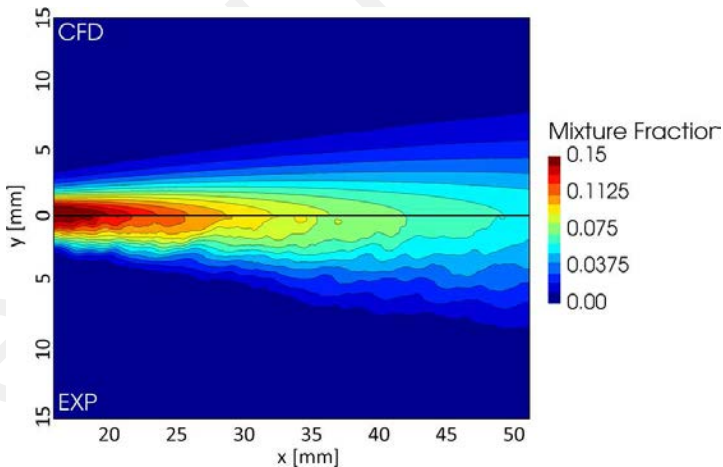


FIG. 18: Mixture fraction contour comparison for Test point 3

7. CONCLUSIONS

In this work, a novel method to deal with evaporation within the ELSA framework has been introduced. The approach, which is based on the formulation of evaporation rates in an implicit manner, has been described with particular attention to the calculation of the equilibrium state

of the system. Firstly, its main advantages with respect to standard explicit methods have been described. Then, a preliminary validation has been carried out on a simplified test case representing a single isolated droplet, in order to analytically confirm the implemented approach. Finally, the ECN dataset has been employed for its assessment.

Three different operating conditions have been tested, comparing vapor distributions and time-dependent penetration of the spray tip. Averaged contours of mixture fraction showed a good agreement with experimental data, in particular when a lower injection velocity has been considered. Moreover, a proper description of the near field of the injector has been pointed out, highlighting the characteristics of the evaporation model in dealing with the dense region of the spray. Ultimately, the obtained results assessed the code capabilities in handling evaporation in a robust and reliable manner.

This work represents a key step in the development of an approach able to account for all the phenomena going from the near-injection region up to a dispersed spray since it represents the link between the liquid phase and the reacting flow field. The proposition and the assessment of a numerical strategy to deal with evaporation all along the atomization process is a significant step towards a unified description of spray flames.

REFERENCES

- Abraham, J. and Pickett, L.M., Computed and Measured Fuel Vapor Distribution in a Diesel Spray, *Atomization Sprays*, vol. **20**, no. 3, pp. 241–250, 2010.
- Abramzon, B. and Sirignano, W., Droplet Vaporization Model for Spray Combustion Calculations, *Int. J. Heat Mass Transf.*, vol. **32**, no. 9, pp. 1605–1618, 1989.
- Andreini, A., Bianchini, C., Puggelli, S., and Demoulin, F., Development of a Turbulent Liquid Flux Model for Eulerian–Eulerian Multiphase Flow Simulations, *Int. J. Multiphase Flow*, vol. **81**, pp. 88–103, 2016.
- Anez, J., Ahmed, A., Hecht, N., Duret, B., Reveillon, J., and Demoulin, F., Eulerian–Lagrangian Spray Atomization Model Coupled with Interface Capturing Method for Diesel Injectors, *Int. J. Multiphase Flow*, vol. **113**, pp. 325–342, 2019.
- Battistoni, M., Som, S., and Powell, C.F., Highly Resolved Eulerian Simulations of Fuel Spray Transients in Single and Multi-Hole Injectors: Nozzle Flow and Near-Exit Dynamics, *Fuel*, vol. **251**, pp. 709–729, 2019.
- Beau, P.A., Modélisation de l’Atomisation d’un Jet Liquide Application Aux Sprays Diesel, PhD, Université de Rouen, France, 2006.
- Bird, G., *Molecular Gas Dynamics and the Direct Simulation of Gas Flows*, Oxford, UK: Oxford University Press, 1994.
- Braun, S., Wieth, L., Holz, S., Dauch, T.F., Keller, M.C., Chaussonnet, G., Gepperth, S., Koch, R., and Bauer, H.J., Numerical Prediction of Air-Assisted Primary Atomization Using Smoothed Particle Hydrodynamics, *Int. J. Multiphase Flow*, vol. **114**, pp. 303–315, 2019.
- Canu, R., Puggelli, S., Essadki, M., Duret, B., Menard, T., Massot, M., Reveillon, J., and Demoulin, F.X., Where Does the Droplet Size Distribution Come from?, *Int. J. Multiphase Flow*, vol. **107**, pp. 230–245, 2018.
- Cengel, Y.A. and Boles, M.A., *Thermodynamics: An Engineering Approach*, 8th ed., New York, NY: McGraw-Hill, 2015.
- Chin, J. and Lefebvre, A., The Role of the Heat-Up Period in Fuel Drop Evaporation, *Int. J. Turbo Jet Engines*, vol. **2**, no. 4, pp. 315–326, 1985.
- Desantes, J.M., Garcia-Oliver, J.M., Pastor, J.M., and Pandal, A., A Comparison of Diesel Sprays CFD

- Modeling Approaches: DDM versus Σ -Y Eulerian Atomization Model, *Atomization Sprays*, vol. **26**, no. 7, pp. 713–737, 2016.
- Drew, D. and Passman, S., *Theory of Multicomponent Fluids*, New York, NY: Springer-Verlag, 1999.
- Duret, B., Luret, G., Reveillon, J., Menard, T., Berlemont, A., and Demoulin, F., DNS Analysis of Turbulent Mixing in Two-Phase Flows, *Int. J. Multiphase Flow*, vol. **40**, pp. 93–105, 2012.
- Duret, B., Canu, R., Reveillon, J., and Demoulin, F.X., A Pressure Based Method for Vaporizing Compressible Two-Phase Flows with Interface Capturing Approach, *Int. J. Multiphase Flow*, vol. **108**, pp. 42–50, 2018.
- Essadki, M., de Chaisemartin, S., Laurent, F., and Massot, M., High Order Moment Model for Polydisperse Evaporating Sprays towards Interfacial Geometry Description, *SIAM J. Appl. Math.*, vol. **78**, no. 4, pp. 2003–2027, 2018.
- Estivalèzes, J.L., Zuzio, D., and DiPierro, B., An Improved Multiscale Eulerian–Lagrangian Method for Simulation of Atomization Process, *Turbulence and Interactions*, Cham, Switzerland: Springer International Publishing, pp. 65–77, 2018.
- Frenklach, M., Method of Moments with Interpolative Closure, *Chem. Eng. Sci.*, vol. **57**, no. 12, pp. 2229–2239, 2002.
- García-Oliver, J.M., Pastor, J.M., Pandal, A., Trask, N., Baldwin, E., and Schmidt, D.P., Diesel Spray CFD Simulations based on the Σ -Y Eulerian Atomization Model, *Atomization Sprays*, vol. **23**, no. 1, pp. 71–95, 2013.
- Gautam, R. and Seider, W.D., Computation of Phase and Chemical Equilibrium: Part I. Local and Constrained Minima in Gibbs Free Energy, *AIChE J.*, vol. **25**, no. 6, pp. 991–999, 1979.
- Haider, A. and Levenspiel, O., Drag Coefficient and Terminal Velocity of Spherical and Nonspherical Particles, *Powder Technol.*, vol. **58**, no. 1, pp. 63–70, 1989.
- Hoyas, S., Gil, A., Margot, X., Khuong-Anh, D., and Ravet, F., Evaluation of the Eulerian–Lagrangian Spray Atomization (ELSA) Model in Spray Simulations: 2D Cases, *Math. Comput. Model.*, vol. **57**, nos. 7–8, pp. 1686–1693, 2013.
- Kastengren, A.L., Tilocco, F.Z., Powell, C.F., Manin, J., Pickett, L.M., Payri, R., and Bazyn, T., Engine Combustion Network (ECN): Measurements of Nozzle Geometry and Hydraulic Behavior, *Atomization Sprays*, vol. **22**, no. 12, pp. 1011–1052, 2012.
- Kinzer, G.D. and Gunn, R., The Evaporation, Temperature and Thermal Relaxation-Time of Freely Falling Waterdrops, *J. Meteorol.*, vol. **8**, no. 2, pp. 71–83, 1951.
- Kösters, A. and Karlsson, A., Modeling of Diesel Fuel Spray Formation in OpenFOAM, *Presentation*, p. 25, 2011.
- Kösters, A. and Karlsson, A., Validation of the VSB2 Spray Model Against Spray A and Spray H, *Atomization Sprays*, vol. **26**, no. 8, pp. 775–798, 2016.
- Kralj, C., Numerical Simulation of Diesel Spray Processes, PhD, University of London, UK, 1995.
- Laurent, F. and Massot, M., Multi-Fluid Modeling of Laminar Polydisperse Spray Flames: Origin, Assumptions and Comparison of Sectional and Sampling Methods, *Combust. Theory Model.*, vol. **5**, no. 4, pp. 537–572, 2001.
- Lebas, R., Menard, T., Beau, P., Berlemont, A., and Demoulin, F., Numerical Simulation of Primary Break-Up and Atomization: DNS and Modeling Study, *Int. J. Multiphase Flow*, vol. **35**, no. 3, pp. 247–260, 2009.
- Lefebvre, A.H. and McDonell, V.G., *Atomization and Sprays*, Boca Raton, FL: CRC Press, 2017.
- Liu, A.B., Mather, D., and Reitz, R.D., Modeling the Effects of Drop Drag and Breakup on Fuel Sprays, *SAE Technical Paper*, SAE International, 1993.
- Ménard, T., Tanguy, S., and Berlemont, A., Coupling Level Set/VOF/Ghost Fluid Methods: Validation and

- Application to 3D Simulation of the Primary Break-Up of a Liquid Jet, *Int. J. Multiphase Flow*, vol. **33**, no. 5, pp. 510–524, 2007.
- Moran, M.J. and Shapiro, H.N., *Fundamentals of Engineering Thermodynamics*, 6th ed., New York, NY: Wiley and Sons, 2009.
- Morsi, S.A. and Alexander, A.J., An Investigation of Particle Trajectories in Two-Phase Flow Systems, *J. Fluid Mech.*, vol. **55**, no. 2, p. 193, 1972.
- Ning, W., Reitz, R.D., Lippert, A.M., and Diwakar, R., Development of a Next-Generation Spray and Atomization Model Using an Eulerian–Lagrangian Methodology, *17th Int. Multidimensional Engine Modeling User’s Group Meeting*, Detroit, MI, April 2007
- O’Rourke, P.J. and Amsden, A.A., The Tab Method for Numerical Calculation of Spray Droplet Breakup, *SAE Technical Paper*, SAE International, 1987.
- Pandal, A., Implementation and Development of an Eulerian Spray Model for CFD Simulations of Diesel Sprays, PhD, Universitat Politècnica de València, Spain, 2016.
- Pilch, M. and Erdman, C., Use of Breakup Time Data and Velocity History Data to Predict the Maximum Size of Stable Fragments for Acceleration-Induced Breakup of a Liquid Drop, *Int. J. Multiphase Flow*, vol. **13**, no. 6, pp. 741–757, 1987.
- Puggelli, S., Palanti, L., Andreini, A., and Demoulin, F., Development of an Evaporation Model for the Dense Spray Region in Eulerian–Eulerian Multiphase Flow Simulations, *28th Conf. on Liquid Atomization and Spray System, (ILASS-Europe)*, Paper No. 4652, 2017.
- Reitz, R.D. and Beale, J.C., Modeling Spray Atomization with the Kelvin–Helmholtz/Rayleigh–Taylor Hybrid Model, *Atomization Sprays*, vol. **9**, no. 6, pp. 623–650, 1999.
- Reynolds, W.C., The Element Potential Method for Chemical Equilibrium Analysis: Implementation in the Interactive Program Stanjan, Tech. Rep., 1986.
- Rueda Villegas, L., Alis, R., Lepilliez, M., and Tanguy, S., A Ghost Fluid/Level Set Method for Boiling Flows and Liquid Evaporation: Application to the Leidenfrost Effect, *J. Comput. Phys.*, vol. **316**, pp. 789–813, 2016.
- Shinjo, J. and Umemura, A., Simulation of Liquid Jet Primary Breakup: Dynamics of Ligament and Droplet Formation, *Int. J. Multiphase Flow*, vol. **36**, no. 7, pp. 513–532, 2010.
- Shinjo, J. and Umemura, A., Surface Instability and Primary Atomization Characteristics of Straight Liquid Jet Sprays, *Int. J. Multiphase Flow*, vol. **37**, no. 10, pp. 1294–1304, 2011.
- Sirignano, W.A., *Fluid Dynamics and Transport of Droplets and Sprays*, Cambridge, UK: Cambridge University Press, 1999.
- Tanguy, S., Ménard, T., and Berlemont, A., A Level Set Method for Vaporizing Two-Phase Flows, *J. Comput. Phys.*, vol. **221**, no. 2, pp. 837–853, 2007.
- Taylor, G.I., The Instability of Liquid Surfaces when Accelerated in a Direction Perpendicular to Their Planes, I, *Proc. R. Soc. London. Ser. A. Math. Phys. Sci.*, vol. **201**, no. 1065, pp. 192–196, 1950.
- Vallet, A. and Borghi, R., Modélisation Eulerienne de L’atomisation d’un Jet Liquide, *Comptes Rendus de l’Académie des Sciences - Series IIB - Mechanics-Physics-Astronomy*, vol. **327**, no. 10, pp. 1015–1020, 1999.
- Williams, F.A., Spray Combustion and Atomization, *Phys. Fluids*, vol. **1**, no. 6, pp. 541–545, 1958.
- Yang, X., Ray, M., Kong, S.C., and Kweon, C.B.M., SPH Simulation of Fuel Drop Impact on Heated Surfaces, *Proc. Combust. Inst.*, vol. **37**, no. 3, pp. 3279–3286, 2019.
- Yuan, C., Laurent, F., and Fox, R., An Extended Quadrature Method of Moments for Population Balance Equations, *J. Aerosol Sci.*, vol. **51**, pp. 1–23, 2012.